The Structure of L-Tyrosine 2,3-Aminomutase from the C-1027 Enediyne Antitumor Antibiotic Biosynthetic Pathway†,‡

Carl V. Christianson,§ Timothy J. Montavon,§ Steven G. Van Lanen,|| Ben Shen,||,⊥,# and Steven D. Bruner*,§

Department of Chemistry, Boston College, Eugene F. Merkert Chemistry Center, Chestnut Hill, Massachusetts 02467, Division of Pharmaceutical Sciences, University of Wisconsin National Cooperative Drug Discovery Group, and Department of Chemistry, University of Wisconsin−Madison, Madison, Wisconsin 53705

Received February 21, 2007; Revised Manuscript Received April 9, 2007

ABSTRACT: The SgcC4 L-tyrosine 2,3-aminomutase (*Sg*TAM) catalyzes the formation of (*S*)-*β*-tyrosine in the biosynthetic pathway of the enediyne antitumor antibiotic C-1027. *Sg*TAM is homologous to the histidine ammonia lyase family of enzymes whose activity is dependent on the methylideneimidazole-5-one (MIO) cofactor. Unlike the lyase enzymes, *Sg*TAM catalyzes additional chemical transformations resulting in an overall stereospecific 1,2-amino shift in the substrate L-tyrosine to generate (*S*)-*β*-tyrosine. Previously, we provided kinetic, spectroscopic, and mutagenesis data supporting the presence of MIO in the active site of *Sg*TAM [Christenson, S. D.; Wu, W.; Spies, A.; Shen, B.; and Toney, M. D. (2003) *Biochemistry 42,* 12708−12718]. Here we report the first X-ray crystal structure of an MIO-containing aminomutase, *Sg*TAM, and confirm the structural homology of *Sg*TAM to ammonia lyases. Comparison of the structure of *Sg*TAM to the L-tyrosine ammonia lyase from *Rhodobacter sphaeroides* provides insight into the structural basis for aminomutase activity. The results show that *Sg*TAM has a closed active site well suited to retain ammonia and minimize the formation of lyase elimination products. The amino acid determinants for substrate recognition and catalysis can be predicted from the structure, setting the framework for detailed mechanistic investigations.

C-1027 belongs to the chromoprotein family of enediyne antitumor antibiotic products that are produced mainly by the actinomycetes (Figure 1A) (*1*). The potent DNA-cleaving ability and unique mechanism of action of these natural products make them promising leads for novel therapeutic agents. Enediynes are produced by complex enzyme pathways containing components of both polyketide and nonribosomal peptide machinery (*2*−*5*). The biosynthetic routes of these molecules are largely convergent, incorporating building blocks derived from amino acids, polyketides, and carbohydrates around a central enediyne core. Three enediynes contain modified *β*-tyrosine moieties as structural components, and the aromatic functionality is predicted to interact with the enediyne and modulate the Bergman cyclization leading to diradical formation and biological activity (*6*). C-1027, produced by *Streptomyces globisporus*, incorporates an (*S*)-3-chloro-5-hydroxy-*β*-tyrosine in its complex architecture (Figure 1A) (*2*). The biosynthetic pathway to this *β*-amino acid begins with the conversion of L-tyrosine to (*S*)-*β*-tyrosine catalyzed by the SgcC4 L-tyrosine 2,3-aminomutase (*Sg*TAM) (*7, 8*).

The aminomutase class of enzymes catalyze the 1,2-shift of substrate amines in a variety of primary and secondary metabolic pathways. In general, characterized aminomutases rely on complex cofactor chemistry, using radical-based mechanisms to perform this difficult transformation (*9*). For example, lysine 2,3-aminomutase is a "radical-SAM" enzyme dependent on *S*-adenosylmethionine (SAM[1]), an iron−sulfur cluster, and pyridoxal 5′-phosphate (PLP) as cofactors (*10*). The mechanism is believed to proceed through a Schiff-base mediated 1,2-shift of a radical intermediate. Other structurally characterized examples of aminomutases use cobalamin and PLP and follow a similar reaction pathway (*11*). Genetic and biochemical characterization of the C-1027 biosynthetic pathway revealed *Sg*TAM, representing a novel class of aminomutase with a catalytic mechanism dependent on the uncommon cofactor 4-methylideneimidazole-5-one (MIO) (Figure 1B), whose essential role in *Sg*TAM catalysis has been supported by kinetic, spectroscopic, and mutagenesis studies (*2, 7, 8*).

† This work was supported in part by funds from Boston College and the Damon Runyon Cancer Research Foundation DRS-41-01 (to S.D.B) and NIH Grant CA78747 (to B.S.). B.S. is a recipient of an NIH Independent Scientist Award (AI51687). S.G.V.L is a recipient of an NIH postdoctoral fellowship (CA1059845).

‡ Coordinates have been deposited within the Protein Data Bank (PDB code 2OHY).

* To whom correspondence should be addressed. Tel: 617-552-2931. Fax: 617-552-2705. E-mail: bruner@bc.edu.

§ Boston College.

|| Division of Pharmaceutical Sciences, University of Wisconsin−Madison.

⊥ University of Wisconsin National Cooperative Drug Discovery Group, University of Wisconsin−Madison.

Department of Chemistry, University of Wisconsin−Madison.

[1] Abbreviations: TAM, tyrosine aminomutase; MIO, methylideneimidazole-5-one; SAM, *S*-adenosylmethionine; PLP, pyridoxal 5′-phosphate; HAL, histidine ammonia lyase; PAL, phenylalanine ammonia lyase; TAL, tyrosine ammonia lyase; LB, Luria−Bertani media; IPTG, isopropyl-*β*-D-thiogalactopyranoside; Ni-NTA, nickel nitrilotriacetic acid; OPA, *o*-phthaldialdehyde; AIP, 2-aminoindan-2-phosphonic acid.

10.1021/bi7003685 CCC: $37.00
Published on Web 05/22/2007

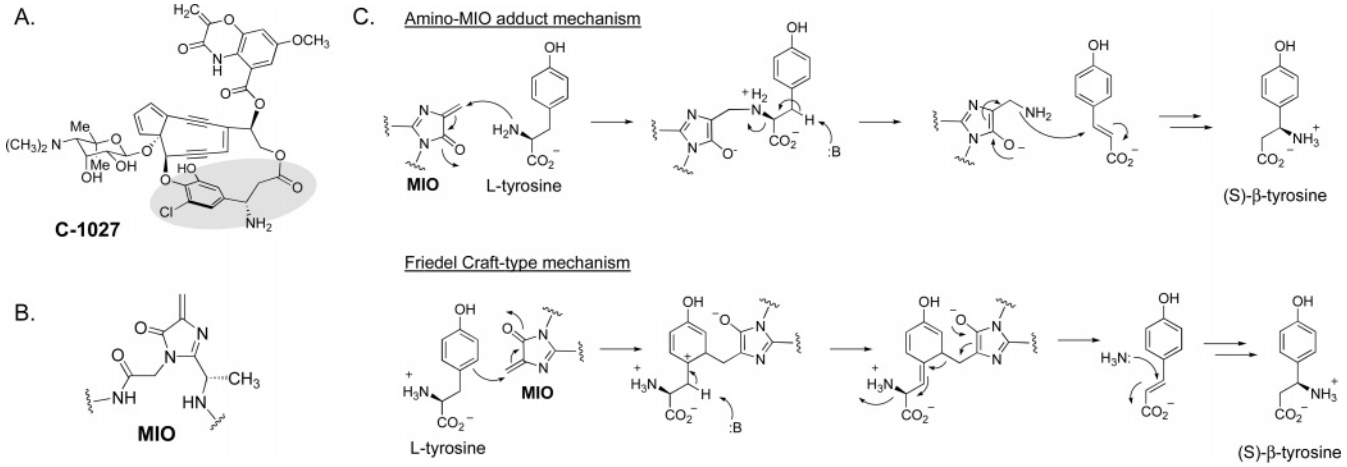

FIGURE 1: (*S*)-*β*-Tyrosine biosynthesis in enediyne natural products. (A) The structure of C-1027 with the (*S*)-*β*-tyrosine moiety highlighted. (B) The structure of the MIO cofactor formed by condensation of an Ala-Ser-Gly motif present in *Sg*TAM. (C) Two reaction pathways for an MIO-based aminomutase based on the proposed mechanistic schemes for MIO-based ammonia lyases.

β-Amino acids are important and useful building blocks in both natural and unnatural peptidic systems (*12*, *13*). Besides enediyne pathways, MIO-based aminomutases are responsible for the synthesis of *β*-amino acids incorporated into other classes of natural products. For example in taxane biosynthesis, a phenylalanine aminomutase is responsible for the formation of a key building block in the taxane side chain (*14*) and the biosynthetic gene cluster of the mixed polyketide/nonribosomal peptide andrimid contains a gene predicted to encode an MIO-based phenylalanine aminomutase (*15*).

The MIO cofactor is formed by the condensation of a conserved Ala-Ser-Gly motif present in the protein backbone (*16*). The self-catalyzed reaction is chemically analogous to the formation of the chromophore present in the green fluorescent protein (*17*). The histidine ammonia lyase (HAL) family of enzymes contains a well-characterized MIO cofactor (*16*). Members of the HAL family catalyze the elimination of ammonia from aromatic α-amino acids, a process important in amino acid catabolism and secondary metabolism (*18*, *19*). Known substrates of MIO-based ammonia lyases include the aromatic amino acids L-tyrosine, L-phenylalanine, and L-histidine. Recently, X-ray structures of several members from this family have been determined including a HAL structure from *Pseudomonas putida* (*20*), phenylalanine ammonia lyase (PAL) structures from *Petroselinum crispum* (*21*) and *Rhodosporidium toruloides* (*22*), and tyrosine ammonia lyase (TAL) from *Rhodobacter sphaeroides* (*23*). The structures reveal a common motif where the monomer subunits are composed largely of α-helices with the MIO cofactor positioned at the termini of multiple helices. The biologically active subunit is tetrameric where the monomers are related by 222 symmetry. The composite active site is at the junction of monomers, and the four catalytic centers each contain amino acid side chains from three of the four subunits.

Two debated mechanisms have been proposed to account for the MIO-catalyzed elimination of ammonia observed in the HAL family (*24*, *25*). The highly electrophilic MIO cofactor is postulated to react with either the aromatic ring (Friedel−Crafts-type mechanism) or the amine of the amino acid substrate (amino−MIO adduct mechanism) (Figure 1C). Both mechanisms lead to acidification of the *β*-hydrogens and subsequent elimination of ammonia to generate the observed α,*β*-unsaturated acid products. Based on sequence homology of *Sg*TAM to the HAL family and predicted conservation of the MIO cofactor, a shared reaction coordinate has been proposed to account for the observed 1,2-amino shift (Figure 1C) (*7*, *8*). In the first step, analogous to ammonia lyases, ammonia is eliminated to generate an intermediate coumarate. Subsequent 1,4-addition of ammonia into this intermediate leads to (*S*)-*β*-tyrosine. Based on this hypothesis, an MIO-based aminomutase must minimally retain ammonia in the active site and activate an intermediate for nucleophilic addition. The structural and mechanistic basis for the differentiation between MIO-based ammonia lyases and aminomutases has not been established.

Here we report the X-ray crystal structure of *Sg*TAM, the first MIO-containing aminomutase to be structurally characterized. The 2.5 Å resolution structure confirms that (i) *Sg*TAM contains an autocatalytically formed MIO cofactor and (ii) MIO-based aminomutases such as *Sg*TAM are structurally homologous to the HAL-family of ammonia lyases. The structural information allows insights into the mechanistic differences between aminomutases and ammonia lyases. Comparisons between *Sg*TAM and a homologous L-tyrosine ammonia lyase are exploited to understand the mechanism of the MIO-based aminomutase activity. The results reveal the structural basis for substrate recognition and catalysis, setting the stage to explore the chemical mechanism employed by this new family of aminomutases. In addition to providing information on the mechanism of (*S*)-*β*-tyrosine formation, this work represents the first structural details into the biosynthetic pathway of the C-1027 enediyne antitumor antibiotics, a proposed target of bioengineering (*1*).

MATERIALS AND METHODS

Enzyme Production. The *sgcC4* expression construct pBS1022 was used to overproduce *Sg*TAM (58 kDa, 539 amino acids) as described previously (*8*). Briefly, pBS1022 was transformed into BL21(DE3) cells and grown in LB media at 37 °C until cell density reached OD = 0.6 (*7*, *8*). Overexpression was induced by adding IPTG (50 *μ*M), followed by overnight incubation at 18 °C. Cells were pelleted by centrifugation and lysed using a French Press

Table 1: X-ray Data Collection and Refinement Statistics[a]

crystal form	primitive orthorhombic
PDB code	2OHY
beam line	NSLS X26C
wavelength	0.9795
space group	$P2_12_12$
cell dimensions (Å)	92.597, 146.178, 75.437
resolution of structure	50.0−2.50 (2.59−2.50)
unique reflections	35786 (3515)
completeness	99.9 (99.7)
redundancy	6.0 (5.9)
$I/\sigma(I)$	18.6 (4.1)
R_{merge} (%)	9.4 (53.4)
monomers per asymmetric unit	2
solvent content (%)	40.39
amino acid residues	1057
no. of non-hydrogen atoms	8021
water molecules	417
$R_{working}/R_{free}$	0.192/0.264
rmsd of bond lengths	0.0057
rmsd of bond angles	1.267
average *B*-factor	29.56

[a] Statistics in the highest data bin are shown in parentheses.

cell disruption system. The enzyme was purified with Ni-NTA affinity resin (Qiagen), followed by cleavage of the N-terminal His_6-tag with the protease thrombin (2 days at 4 °C). Further purification was performed with a HiTrap-Q ion exchange column followed by a Superdex 200 gel filtration column (GE Biosciences).

*Crystallization and Data Collection. Sg*TAM was crystallized by the hanging drop vapor diffusion method at 4 °C. *Sg*TAM (1.5 μL of 10 mg/mL in 20 mM Tris-HCl, 1 mM β-mercaptoethanol, and 100 mM NaCl, pH 7.5) was mixed with 1.5 μL of reservoir solution (4.4 M sodium formate, 100 mM trimethylamine *N*-oxide). Needle shaped crystals appeared within 2 days and were allowed to continue growth for approximately 1 week. Crystals were transferred to a cryoprotectant solution of the reservoir solution with 20% glycerol and briefly soaked before being flash frozen in liquid nitrogen. X-ray diffraction data was collected on the X26C beamline at the National Synchrotron Light Source at Brookhaven National Laboratory on an ADSC Quantum 4 CCD detector at 100 K. Diffraction intensities were indexed, integrated, and scaled with HKL2000 (*26*) as summarized in Table 1. The crystal belongs to the space group $P2_12_12$, with unit cell dimensions $a = 92.6$ Å, $b = 146.2$ Å, $c = 75.4$ Å and $\alpha = \beta = \gamma = 90°$.

Structure Determination. The initial structure solution was obtained by a molecular replacement approach. From sequence analysis of MIO-based lyases, histidine ammonia lyase (pdb code: 1B8F) was chosen as an initial search model based on homology to *Sg*TAM. A polyalanine model of the histidine ammonia lyase monomer was used to generate initial solutions using the programs AMORE and MOLREP (*27*, *28*). Multiple solutions were screened and evaluated based on the ability to form symmetry-related tetramers consistent with the biological unit.

Model Building and Refinement. Model building was performed with the program COOT (*29*) using the initial polyalanine HAL solution as a guide. Refinement cycles and generation of electron density maps were done using the CNS suite of programs (*30*). The parameter and protein topology files were modified to incorporate the MIO moiety into the protein backbone structure. Cycles of rigid body refinement, simulated annealing guided by σ-weighted composite omit maps were carried out until the *R*-values were no longer improved to any extent. The program PyMOL (Delano Scientific, San Carlos, CA) was used to generate graphic images.

Biochemical Assay of SgTAM. The biochemical activity of *Sg*TAM was confirmed by using an HPLC based assay with modifications (*8*). Reactions were performed at 25 °C with 100 μM L-tyrosine in 20 mM Tris-HCl, 100 mM NaCl, 100 μM β-mercaptoethanol, and 0.5 mg/mL of *Sg*TAM at pH 7.5. Aliquots from the reaction were quenched by the addition of 0.2 M HCl until the pH reached 2.0. The enzyme was then removed by centrifugation. The supernatant was returned to pH 9.0 by the addition of 0.25 M NaOH. *o*-Phthaldialdehyde (OPA) derivatives of the reaction mixture were obtained by mixing an equal volume of OPA reagent (16 mg OPA in 200 μL of ethanol, 44 μL of β-mercaptoethanol, and 17 mL of 100 mM sodium borate pH 10.7) with neutralized aliquots for 1 min followed by the addition of 1% v/v acetic acid. After derivation, the mixture was analyzed by HPLC on a C18 column using gradients of eluent A (5 mM sodium acetate (pH 5.7) in 95:5 H_2O/THF) and eluent B (5 mM sodium acetate (pH 5.7) in 45:45:10 methanol/acetonitrile/water).

RESULTS

*Crystallization and Structure Determination of the L-Tyrosine Aminomutase, SgTAM. Sg*TAM from the C-1027 biosynthetic pathway was overproduced in *Escherichia coli* and purified as described previously (*7*, *8*). For crystallization, the N-terminal His_6-tag was removed via proteolysis, and the resultant enzyme was purified using two chromatography steps as described in the Materials and Methods section. The production of active protein was monitored by employing an HPLC-based biochemical assay at various points during the purification and crystallization (*7*, *8*). *Sg*TAM crystallized in the space group $P2_12_12$ with two 58 kDa monomers per asymmetric unit. Initial phase information used to solve the structure was obtained using molecular replacement techniques. L-Histidine ammonia lyase from *P. putida* (36% sequence identity) was selected as a search model based on predicted common structural motifs (see Figure 2) (*20*). A polyalanine model of HAL monomer was used to generate initial phase information to solve the structure. The correct solution had a preliminary *R*-value of 0.51. The model of *Sg*TAM was built into the density maps and refined to 2.5 Å resolution. The two monomers of the asymmetric unit are very similar with a root-mean-squared difference between equivalent backbone atoms of 1.17 Å. The final model contains residues 12−539 and 11−539 in the two respective monomers.

The Overall Structure of SgTAM. The structure of *Sg*TAM (Figure 3A) displays structural homology to the core structures of ammonia lyases. Symmetry operations in the unit cell generate a head-to-tail dimer of dimers related by 222 point symmetry. The active, biological unit of *Sg*TAM is assigned as a tetramer based on homology with the HAL superfamily of ammonia lyases. The total buried surface area is significant and calculated to be 8400 Å^2 per *Sg*TAM monomer. The overall structure is largely α-helical with most helices running along the long axis of the monomer structure

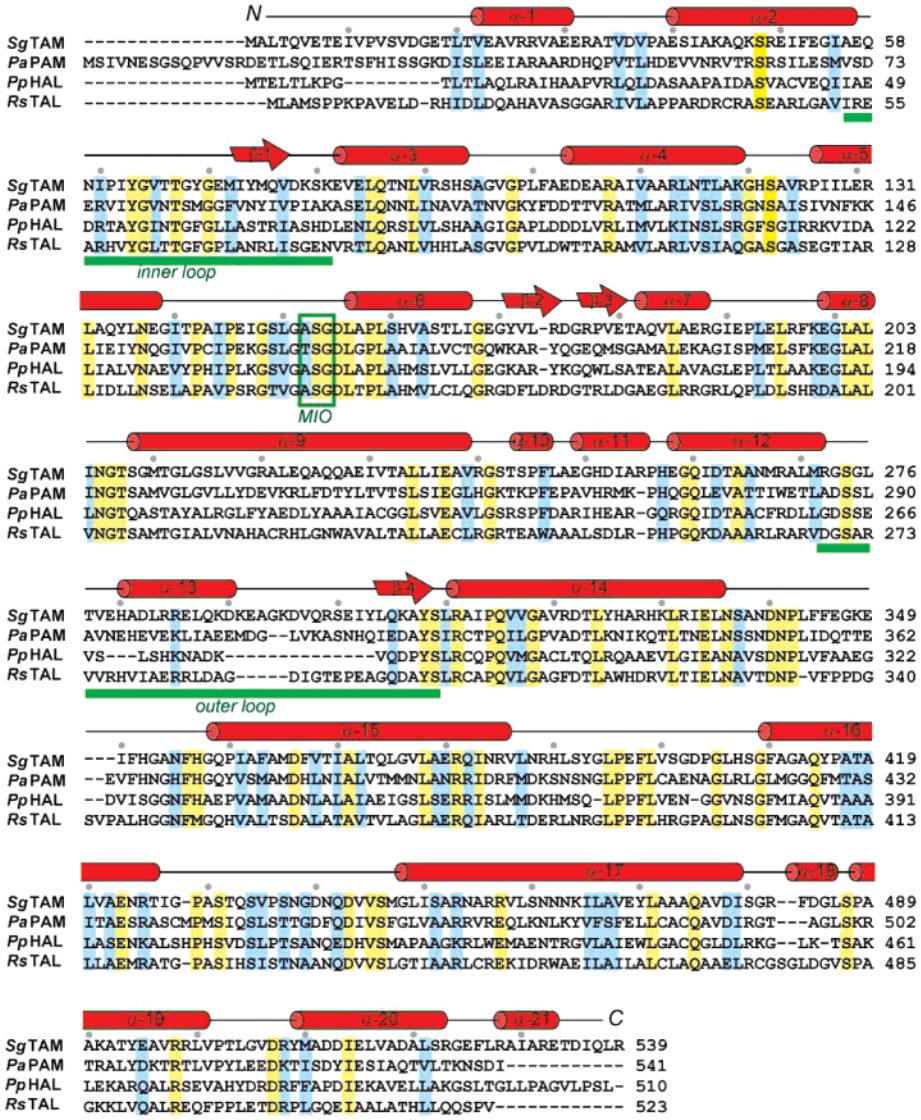

FIGURE 2: Sequence alignment of representative MIO-based aminomutases and ammonia lyases. The secondary structure corresponding to *Sg*TAM is illustrated above the sequences. The three residues that form the active site MIO are boxed in green, and the inner and outer loop regions are indicated below the sequences. Sequences were aligned using the ClustalW pairwise alignment protocol. Abbreviations used: *Sg*TAM, *S. globisporus* L-tyrosine aminomutase; *Pa*PAM, *P. agglomerans* L-phenylalanine aminomutase; *Pp*HAL, *P. putida* L-histidine ammonia lyase; *Rs*TAL, *R. sphaeroides* L-tyrosine ammonia lyase.

(Figure 3B). There is a single β-sheet in the monomer, composed of two short strands. A second β-sheet forms in the tetramer from two β-strands in adjacent monomers. These two short strands precede helices α-3 and α-15 in the monomer structure. The active site is located close to one end of the monomer structure near the termini of several α-helices and is situated at the positive end of several helix dipoles. Specifically the ends of helices α-6, α-9, α-15, and α-17 are directed at the MIO cofactor, a feature common in MIO-based ammonia lyases (*22*).

The Active Site Containing MIO. The MIO cofactor in *Sg*TAM is formed by the self-condensation of Ala152, Ser153, and Gly154. The MIO is clearly formed in our structure based on examination of the electron density maps (Figure 4A). The two active sites present in our asymmetric unit are very similar in both the orientation of the MIO and adjacent side chains. From examination of the composite omit electron density maps, orphan density is evident at higher sigma levels contiguous with the methylidene group of the MIO cofactor. This suggests partial occupancy of a small molecule nucleophile complexed to the electrophilic MIO. It has been observed in previous structures of ammonia lyases that nucleophiles can react with the MIO. For example, in the presence of cysteine, a covalent complex of the histidine ammonia lyases is formed with the thiol group of the amino acid (*31*). β-Mercaptoethanol was present during our enzyme purification steps, and this thiol models well into the extra electron density as a covalent adduct with the MIO cofactor. The addition of β-mercaptoethanol into the MIO appears to be reversible as the enzyme retains biochemical activity under the conditions utilized during purification (Figure 4B). Though the pH used is not optimal for enzyme activity, turnover is still observed in a 120 min reaction. In addition, the published biochemical conditions contained dithiothreitol, which like β-mercaptoethanol, has the ability to react with the MIO. We cannot, however, rule out the possibility that the observed activity results from the enzyme fraction with an unmodified MIO.

The active site is located at the subunit junction of the *Sg*TAM tetramer. Amino acid side chains from three of the

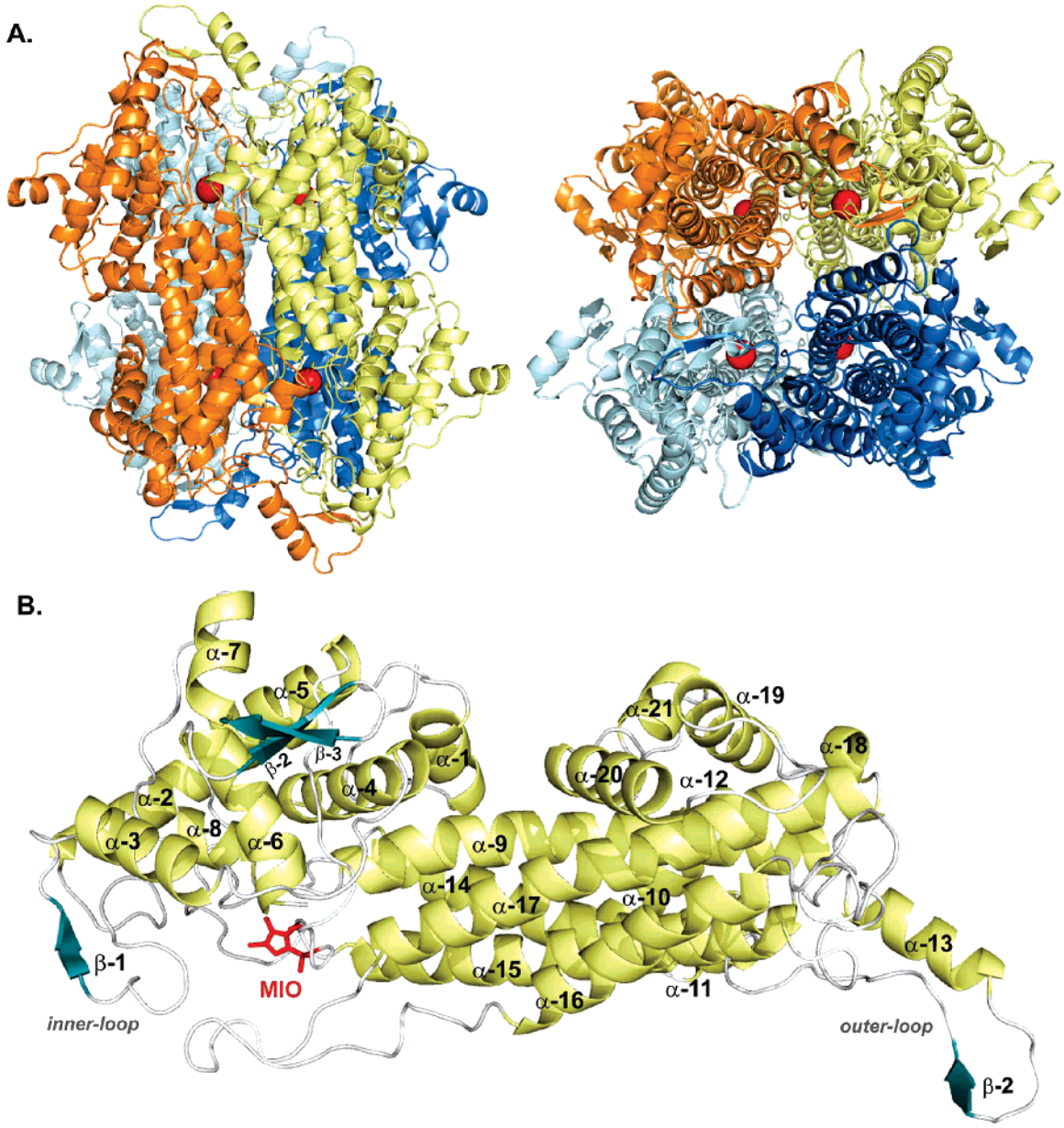

FIGURE 3: The X-ray structure of the L-tyrosine 2,3-aminomutase, *Sg*TAM. (A) Structure of the tetramer with each monomer distinctly colored. The views are looking along the two axes of symmetry. The location of the active site is indicated by the four red spheres. (B) Structure of the *Sg*TAM monomer. The secondary structure elements are labeled. The MIO cofactor is colored in red, and the loop regions surrounding the active site are indicated.

four monomers come together to generate a composite active site. The area immediately surrounding the MIO is composed largely of aromatic side chains, including Tyr63 and His93 from the A monomer, Tyr308 from the B monomer, and Tyr415 from the C monomer (the A monomer is defined as the chain containing the MIO cofactor) (Figure 4C). In addition, the polar side chains of Asn205, Gln438, and Gln442 from the A chain and Arg311 from the B chain are in proximity to the MIO center (Figure 4C). Residues implicated in MIO formation for the HAL ammonia lyases are structurally conserved in *Sg*TAM (*32*). For example, Phe356 corresponds to Phe329 in HAL, a residue proposed to play a key role in the autocatalytic formation of MIO.

The active site of *Sg*TAM with bound β-mercaptoethanol is in a "closed" conformation as defined by the structures of ammonia lyases. Based on previous structural work the "open" form predominates without substrate or analogues in the active site (*20*−*23*, *31*, *33*). Two protein loops cover the active site in the HAL enzyme family and are proposed to play important roles in substrate binding and catalysis (*34*). An inner loop contributes side chain functionality to the active site, and an outer loop further covers and protects the reactive active site center. In the structure of *Sg*TAM, the inner loop corresponds to residues 56−84 and the outer loop to residues 271−308 (Figure 2 and 3B). The inner loop is close in proximity to the MIO, placing the 4-OH of Tyr63 within 5.6 Å of the methylidene carbon of MIO. This tyrosine forms a hydrogen bond with Gly70, and both residues are conserved in all MIO-containing homologues. As compared to the tyrosine ammonia lyase from *R. sphaeroides* (*Rs*TAL) and other ammonia lyase structures, the active site loops of *Sg*TAM are in general longer (Figure 2) and contain more secondary structure elements. As illustrated in Figure 3B,

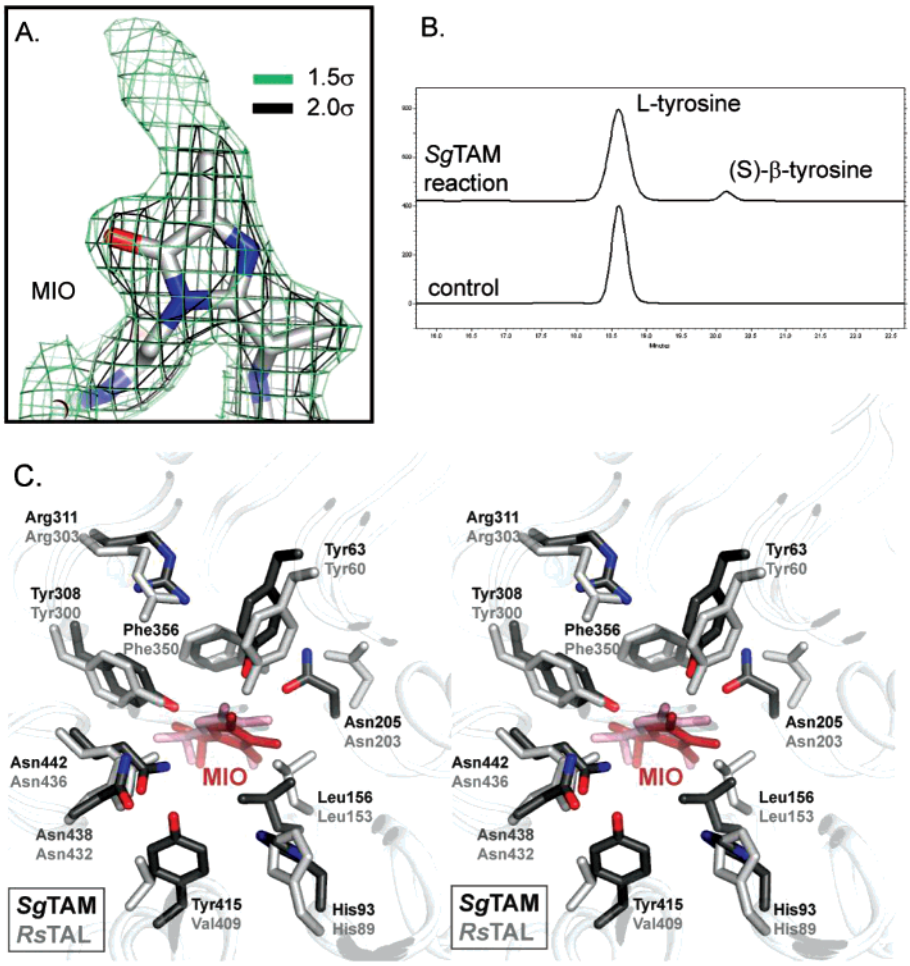

FIGURE 4: The active site of *Sg*TAM. (A) Electron density map around the MIO cofactor. The map is scaled at 2.0σ (black) and 1.5σ (green). (B) HPLC trace showing the conversion of L-tyrosine to (*S*)-β-tyrosine catalyzed by *Sg*TAM under the crystallization conditions. The OPA-amino acid derivatives are monitored at 335 nm on a C18 reverse-phase column. (C) Superposition of the active sites of *Sg*TAM with the L-tyrosine ammonia lyase, *Rs*TAL (pdb# 2O6Y). The stereoview showing the amino acid side chains in close proximity to the MIO cofactor. Residues and labels corresponding to *Sg*TAM are colored dark gray and *Rs*TAL light gray.

an α-helix (α-13) is formed in the outer loop and a short two-strand β-sheet forms between the outer loop of one monomer and the inner loop of another. These structural elements contribute to an ordered and closed active site as discussed below.

Comparison of the SgTAM Active Site with L-Tyrosine Ammonia Lyase. The L-tyrosine ammonia lyase *Rs*TAL shares the same substrate as *Sg*TAM, and the enzymes are 38% identical at the amino acid level (*23*). The overlay of the active site of *Sg*TAM and the tyrosine ammonia lyase from *R. sphaeroides* (*Rs*TAL; pdb code 2O6Y) is shown in Figure 4C. Overall the active sites exhibit a very similar architecture. The MIO cofactor is in approximately the same orientation in each of the structures, and amino acid side chains surrounding the MIO are largely conserved among the two structures. The single prominent difference in the side chains is the presence of Tyr415 in *Sg*TAM where in *Rs*TAL this position is occupied by Val409.

Restricted Active Site of SgTAM. Translating the general reaction mechanism of ammonia lyases to *Sg*TAM predicts the production of the intermediates coumarate and free ammonia (Figure 1C). Biochemical experiments support this reaction pathway as coumarate is a product of *Sg*TAM reaction at extended reaction times (*8*). Based on this mechanism, an efficient aminomutase would be expected to retain free ammonia in the active site and sequester it in the neutral, nucleophilic state. From comparison of the active sites of *Sg*TAM with *Rs*TAL (and other ammonia lyases), the active site of the aminomutase lacks accessibility to the solvent as present in ammonia lyases (Figure 5). The active sites of ammonia lyases are accessible to bulk solvent through an opening in the loops forming a small channel (Figure 5B). Solvent accessibility from the MIO to the protein surface is not apparent in *Sg*TAM (Figure 5A). Two residues appear particularly important in blocking access to the active site. Tyr303 and Glu71 form a hydrogen-bonding interaction across the channel, an interaction not present in *Rs*TAL or other lyase structures. As illustrated, in ammonia lyases the MIO cofactor is visible from the surface through a small channel (Figure 5D). This feature could facilitate diffusion of ammonia/ammonium out of the lyase active site. The same views of *Sg*TAM suggest an enclosed active site (Figure 5C). In addition, as discussed above, the inner and outer loops of *Sg*TAM contain additional secondary structure elements not present in ammonia lyase structures further shielding the active site with ordered loops (Figures 5E and 5F).

Recognition of the Substrate L-Tyrosine in SgTAM. Based on the strong structural homology to L-tyrosine ammonia lyase, the residues involved in substrate recognition in *Sg*TAM can be predicted. A model (Figure 6) of L-tyrosine

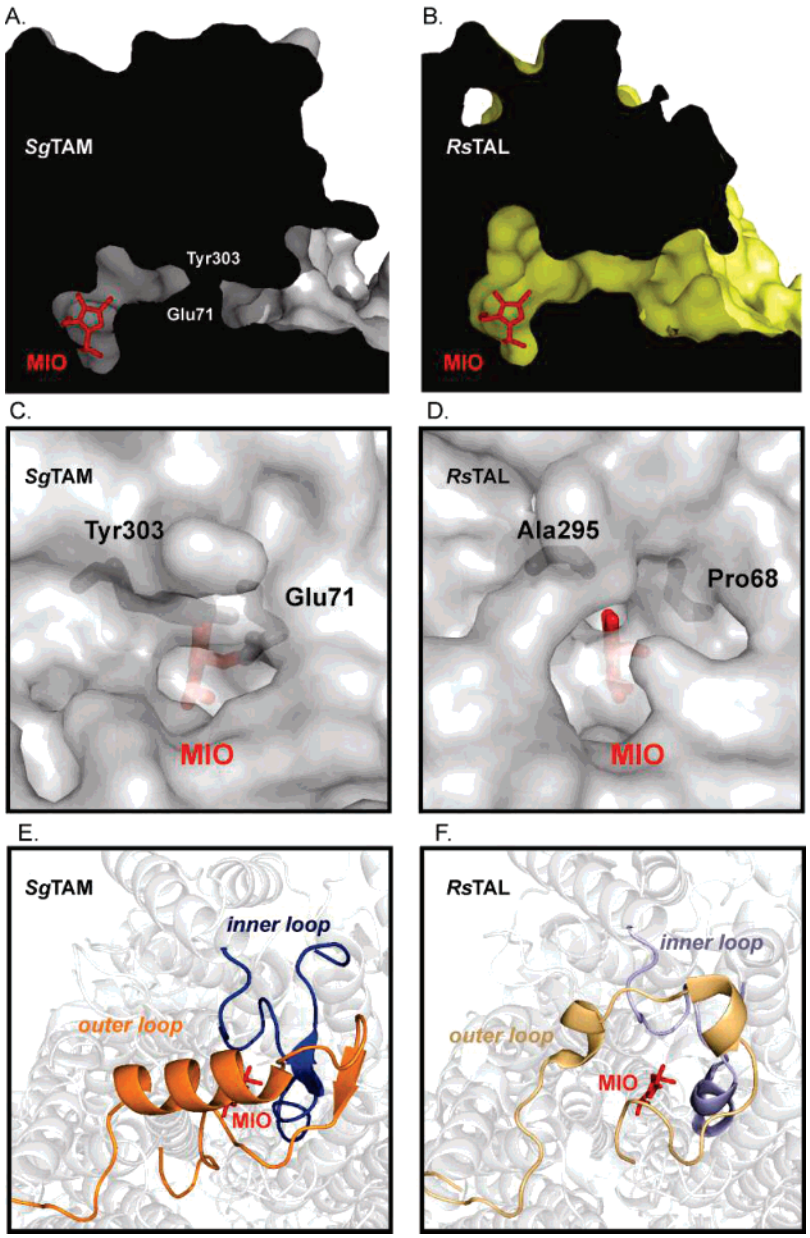

FIGURE 5: Accessibility of the active site of *Sg*TAM as compared with the tyrosine ammonia lyase *Rs*TAL. (A and B) Cutaway view of the area leading from the surface to the MIO. The solvent accessible surface was generated using a probe sphere radius of 1.4 Å. The MIO cofactor is colored red in licorice representation. (C and D) View of the active site from the surface. Key side chains are illustrated. (E and F) Ribbon cartoon representation comparing the loop regions of *Sg*TAM with *Rs*TAL.

bound in the active site of *Sg*TAM was prepared by superposition of the *Rs*TAL/2-aminoindan-2-phosphonic acid (AIP) structure (pdb code 2O7E) (*23*, *35*) and overlay of L-tyrosine on to the position of AIP with minimal modification. We chose to model L-tyrosine as the amine complex with MIO based on the significant homology and structural overlap with the *Rs*TAL/AIP structure. The binding mode is consistent with the amino−MIO adduct mechanism (Figure 1C) and is in agreement with recent structural and modeling work on phenylalanine ammonia lyase (*23*, *36*). L-Tyrosine fits well into the aminomutase active site, and the model confirms amino acid residues important for chemistry and recognition. Notably, the position of His89 (in *Rs*TAL) has been established as a key recognition element in ammonia lyases (*23*, *36*). Mutation of this side chain allows alteration of the preferred amino acid substrate. In *Sg*TAM, this position (His93) is also structurally conserved and the 4-OH of the modeled substrate L-tyrosine is within hydrogen-bonding distance of the histidine. Tyr415 is also within hydrogen bond distance of the substrate 4-OH, indicating a possible role for this side chain. Residues corresponding to Tyr415 are not present in *Rs*TAL or other ammonia lyases. Additional conserved residues in *Sg*TAM that can be predicted to interact with the substrate are Arg311 and Asn205, both in the proper position to interact with the carboxylate of the substrate amino acid.

DISCUSSION

The conversion of α-amino acids to *β*-amino acids via a 1,2-amino shift is a chemically challenging transformation. Characterized examples of aminomutases utilize multicofactor metalloenzymes and accomplish the chemistry using radical intermediates. The SgcC4 L-tyrosine 2,3-aminomutase *Sg*TAM from the enediyne C-1027 biosynthetic pathway in

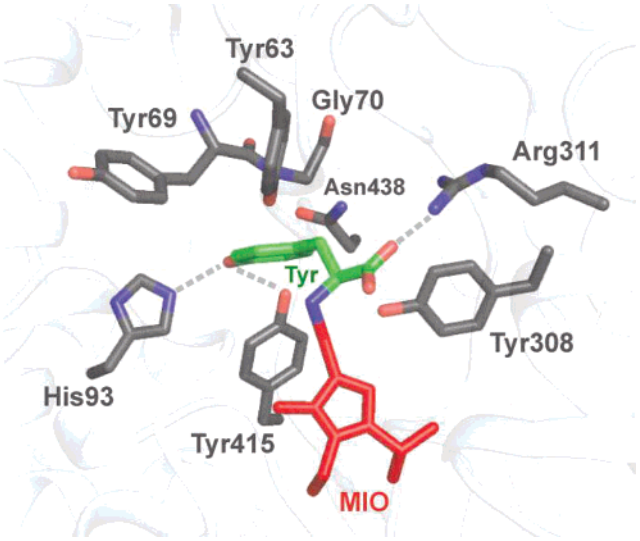

FIGURE 6: Model of the substrate L-tyrosine bound in the active site of *Sg*TAM. Based on the high structure homology with *Rs*TAL, the substrate was modeled into the *Sg*TAM structure by superposition of L-tyrosine with the bound analogue in the AIP/*Rs*TAL co-complex (pdb# 2O7E).

S. globisporus represents a novel class of aminomutase not dependent on metals or complex cofactor chemistry. This enzyme family contains the uncommon MIO cofactor, a functionality previously characterized in aromatic amino acid lyases. The strong sequence and structural homology between MIO-based aminomutases and ammonia lyases suggests a common catalytic pathway. Following this general reaction scheme, an MIO-based L-tyrosine aminomutase must perform the lyase chemistry followed by re-addition of ammonia stereospecifically into coumarate to give (*S*)-β-tyrosine. The second half of the proposed reaction scheme is mechanistically challenging as a coumarate intermediate is a poor acceptor for nucleophilic addition and the enzyme must also retain ammonia in the neutral, deprotonated state. To address the structural basis for the mechanism of MIO-based aminomutases, we have solved the X-ray crystal structure of *Sg*TAM. The structure of *Sg*TAM confirms the structural homology of all characterized MIO-containing enzymes.

To gain insight in the structural determinants for the aminomutase chemistry we have compared the structure of *Sg*TAM with the recently solved structure of tyrosine ammonia lyase, *Rs*TAL (*23*). The two enzymes are highly homologous at both the level of primary sequence and structure. The substrate for the two enzymes is the same; however *Sg*TAM is able to perform an additional chemical step leading to formation of (*S*)-β-tyrosine. The active sites of the two enzymes are remarkably similar (Figure 4C), with a majority of the side chains in approximately the same location. This overlap is independent of the presence or absence of substrate or analogues in the binding pocket suggesting a similar binding mode for L-tyrosine. Only one residue (position 415 in *Sg*TAM) differs significantly in the region of the active site proximal to the MIO. Significant differences between *Sg*TAM and ammonia lyases are evident in the protein loops surrounding the active site. These loop regions are predicted to play roles in shielding the reactive MIO center and substrate binding (*23, 34*). In the structure of *Sg*TAM, two loops form an enclosed active site with limited accessibility to bulk solvent. This is analogous to the "closed" active sites observed in ammonia lyase structures, a feature normally associated with substrate or product binding. The loops in *Sg*TAM contain more pronounced secondary structural elements as compared to the lyase structures (Figures 5E and 5F). Two residues in *Sg*TAM, one coming from each of the active site loops, block an active site channel present in ammonia lyases. Overall, the function of the active site loops in *Sg*TAM could prevent ammonia from leaving the active site, a minimal prerequisite to differentiate an aminomutase from an ammonia lyase.

Exploiting the structural similarity of *Sg*TAM with the L-tyrosine ammonia lyase *Rs*TAL, we modeled the substrate L-tyrosine into the active site of *Sg*TAM (Figure 6). The L-tyrosine is modeled bound to the MIO through the amino group and supports the identity of the residues important for substrate recognition. In particular, His93 is well-positioned to form a hydrogen bond with the 4-OH of substrate L-tyrosine. As experimentally determined for ammonia lyases, the position of His93 is likely a key determinant in substrate specificity in aminomutases. In our structure of *Sg*TAM, β-mercaptoethanol is, at least partially, complexed to the MIO cofactor. The hydroxyl group of the conjugated β-mercaptoethanol forms a hydrogen bond with His93 in a similar position to that proposed for the substrate L-tyrosine in *Rs*TAL (*23*). This model is consistent with the proposed function of His93 as a hydrogen bond acceptor and key determinant for selectivity. The homologous L-phenylalanine aminomutase from *Pantoea agglomerans* (Figure 2) lacks hydrogen-bonding functionality (Val108 at this position). The one significant difference between *Sg*TAM and *Rs*TAL in the area immediately around the active site is at position 415 where *Sg*TAM has a tyrosine. The importance of this residue in enzyme activity has not been established, but Tyr415 is within hydrogen bond distance of the modeled substrate L-tyrosine suggesting a role in substrate recognition and binding. Consistent with this observation, the L-tyrosine Michaelis constant (K_M) for *Sg*TAM is ~3 times lower than that measured for *Rs*TAL (*8, 23*). Additional residues implicated in substrate recognition by ammonia lyases likely serve similar roles in *Sg*TAM. These include Arg311 and Asn205 which both model in position to interact with the carboxylate of the substrate amino acid.

The chemical mechanism of MIO-based enzymes is actively debated and has not entirely been resolved (*24*). A large amount of biochemical, structural, and model system approaches have focused on two alternate roles where the MIO cofactor activates the aromatic ring or the amino group of the amino acid substrate (Figure 1C). The rationale in both cases is to acidify the substrate β-protons to allow deprotonation and elimination of ammonia. Following the reaction scheme of lyases, an MIO-based aminomutase faces the additional challenge of catalyzing the coupling of ammonia into the conjugated coumarate intermediate. Any mechanistic hypothesis requires abstraction of the β-proton/hydrogen from L-tyrosine. The best candidate for a catalytic residue in *Sg*TAM to play this role is Tyr63. This tyrosine forms a hydrogen bond with the backbone of Gly70, and both residues are conserved at this position in all MIO-based ammonia lyases and aminomutases. Tyrosine 308 is also positioned near the MIO in the active site and its 4-OH models close to the α-hydrogen of the substrate L-tyrosine.

Tyr63 and Tyr308 are reasonable candidates to assist in the transfer of hydrogen atom from the β- to α-position in tyrosine as required by the aminomutase chemistry (Figure 6). The precise role of the MIO cofactor in the chemistry of aminomutases remains to be elucidated. The small number of characterized MIO-containing enzymes has limited the generation of a general hypothesis into the precise role of the cofactor. This is especially apparent when the mechanistic theories are translated to the chemistry of aminomutases. Questions related to the mechanistic details of the 1,2-amino shift catalyzed by *Sg*TAM are the subject of ongoing work in our laboratory.

ACKNOWLEDGMENT

We thank Dr. Y. Li, Institute of Medicinal Biotechnology, Chinese Academy of Medical Sciences, Beijing, China, for the C-1027-producing *S. globisporus* strain, and K. Steiglitz for assistance with the initial structure solution along with A. Heroux and the staff at the Brookhaven NSLS PXRR for assistance with X-ray data collection. We are grateful to L. McLaughlin for comments on the manuscript, and members of the Bruner laboratory for helpful discussions.

REFERENCES

1. Shen, B., Liu, W., and Nonaka, K. (2003) Enediyne natural products: biosynthesis and prospect towards engineering novel antitumor agents, *Curr. Med. Chem. 10*, 2317−2325.
2. Liu, W., Christenson, S. D., Standage, S., and Shen, B. (2002) Biosynthesis of the enediyne antitumor antibiotic C-1027, *Science 297*, 1170−1173.
3. Ahlert, J., Shepard, E., Lomovskaya, N., Zazopoulos, E., Staffa, A., Bachmann, B. O., Huang, K., Fonstein, L., Czisny, A., Whitwam, R. E., Farnet, C. M., and Thorson, J. S. (2002) The calicheamicin gene cluster and its iterative type I enediyne PKS, *Science 297*, 1173−1176.
4. Liu, W., Nonaka, K., Nie, L., Zhang, J., Christenson, S. D., Bae, J., Van Lanen, S. G., Zazopoulos, E., Farnet, C. M., Yang, C. F., and Shen, B. (2005) The neocarzinostatin biosynthetic gene cluster from *Streptomyces carzinostaticus* ATCC 15944 involving two iterative type I polyketide synthases, *Chem. Biol. 12*, 293−302.
5. Liu, W., Ahlert, J., Gao, Q., Wendt-Pienkowski, E., Shen, B., and Thorson, J. S. (2003) Rapid PCR amplification of minimal enediyne polyketide synthase cassettes leads to a predictive familial classification model, *Proc. Natl. Acad. Sci U.S.A. 100*, 11959−11963.
6. Okuno, Y., Iwashita, T., and Sugiura, Y. (2000) Structural basis for reaction mechanism and drug delivery system of chromoprotein antitumor antibiotic C-1027, *J. Am. Chem. Soc. 122*, 6848−6854.
7. Christenson, S. D., Liu, W., Toney, M. D., and Shen, B. (2003) A novel 4-methylideneimidazole-5-one-containing tyrosine aminomutase in enediyne antitumor antibiotic C-1027 biosynthesis, *J. Am. Chem. Soc. 125*, 6062−6063.
8. Christenson, S. D., Wu, W., Spies, M. A., Shen, B., and Toney, M. D. (2003) Kinetic analysis of the 4-methylideneimidazole-5-one-containing tyrosine aminomutase in enediyne antitumor antibiotic C-1027 biosynthesis, *Biochemistry 42*, 12708−12718.
9. Wetmore, S. D., Smith, D. M., and Radom, L. (2001) Enzyme catalysis of 1,2-amino shifts: the cooperative action of B6, B12, and aminomutases, *J. Am. Chem. Soc. 123*, 8678−8689.
10. Lepore, B. W., Ruzicka, F. J., Frey, P. A., and Ringe, D. (2005) The X-ray crystal structure of lysine-2,3-aminomutase from *Clostridium subterminale*, *Proc. Natl. Acad. Sci. U.S.A. 102*, 13819−13824.
11. Berkovitch, F., Behshad, E., Tang, K. H., Enns, E. A., Frey, P. A., and Drennan, C. L. (2004) A locking mechanism preventing radical damage in the absence of substrate, as revealed by the x-ray structure of lysine 5,6-aminomutase, *Proc. Natl. Acad. Sci. U.S.A. 101*, 15870−15875.
12. Lelais, G., and Seebach, D. (2004) β-amino acids-syntheses, occurrence in natural products, and components of β-peptides, *Biopolymers 76*, 206−243.
13. Cheng, R. P., Gellman, S. H., and DeGrado, W. F. (2001) β-Peptides: from structure to function, *Chem. Rev. 101*, 3219−3232.
14. Walker, K. D., Klettke, K., Akiyama, T., and Croteau, R. (2004) Cloning, heterologous expression, and characterization of a phenylalanine aminomutase involved in Taxol biosynthesis, *J. Biol. Chem. 279*, 53947−53954.
15. Jin, M., Fischbach, M. A., and Clardy, J. (2006) A biosynthetic gene cluster for the acetyl-CoA carboxylase inhibitor andrimid, *J. Am. Chem. Soc. 128*, 10660−10661.
16. Retey, J. (2003) Discovery and role of methylidene imidazolone, a highly electrophilic prosthetic group, *Biochim. Biophys. Acta 1647*, 179−184.
17. Barondeau, D. P., Kassmann, C. J., Tainer, J. A., and Getzoff, E. D. (2005) Understanding GFP chromophore biosynthesis: controlling backbone cyclization and modifying post-translational chemistry, *Biochemistry 44*, 1960−1970.
18. Winkel-Shirley, B. (2001) Flavonoid biosynthesis. A colorful model for genetics, biochemistry, cell biology, and biotechnology, *Plant Physiol. 126*, 485−493.
19. Klepp, J., Fallert-Muller, A., Grimm, K., Hull, W. E., and Retey, J. (1990) Mechanism of action of urocanase. Specific ^{13}C-labelling of the prosthetic NAD^+ and revision of the structure of its adduct with imidazolylpropionate, *Eur. J. Biochem. 192*, 669−676.
20. Schwede, T. F., Retey, J., and Schulz, G. E. (1999) Crystal structure of histidine ammonia-lyase revealing a novel polypeptide modification as the catalytic electrophile, *Biochemistry 38*, 5355−5361.
21. Ritter, H., and Schulz, G. E. (2004) Structural basis for the entrance into the phenylpropanoid metabolism catalyzed by phenylalanine ammonia-lyase, *Plant Cell 16*, 3426−3436.
22. Calabrese, J. C., Jordan, D. B., Boodhoo, A., Sariaslani, S., and Vannelli, T. (2004) Crystal structure of phenylalanine ammonia lyase: multiple helix dipoles implicated in catalysis, *Biochemistry 43*, 11403−11416.
23. Louie, G. V., Bowman, M. E., Moffitt, M. C., Baiga, T. J., Moore, B. S., and Noel, J. P. (2006) Structural determinants and modulation of substrate specificity in phenylalanine-tyrosine ammonia-lyases, *Chem. Biol. 13*, 1327−1338.
24. Poppe, L., and Retey, J. (2005) Friedel-Crafts-type mechanism for the enzymatic elimination of ammonia from histidine and phenylalanine, *Angew. Chem., Int. Ed. 44*, 3668−3688.
25. Hermes, J. D., Weiss, P. M., and Cleland, W. W. (1985) Use of nitrogen-15 and deuterium isotope effects to determine the chemical mechanism of phenylalanine ammonia-lyase, *Biochemistry 24*, 2959−2967.
26. Otwinowski, Z., and Minor, W. (1997) Processing of X-ray Diffraction Data Collected in Oscillation Mode, in *Methods in Enzymology: Macromolecular Crystallography, part A* (Carter, C. W., Jr., and Sweet, R. M., Eds.) pp 307−326, Academic Press, New York.
27. COLLABORATIVE COMPUTATIONAL PROJECT, N. (1994) The CCP4 Suite: Programs for Protein Crystallography, *Acta Crystallogr., Sect. D: Biol. Crystallogr. 50*, 760−763.
28. Vagin, A., and Teplyakov, A. (1997) MOLREP: an automated program for molecular replacement, *J. Appl. Crystallogr. 30*, 1022−1025.
29. Emsley, P., and Cowtan, K. (2004) Coot: model-building tools for molecular graphics, *Acta Crystallogr., Sect. D: Biol. Crystallogr. 60*, 2126−2132.
30. Brunger, A. T., Adams, P. D., Clore, G. M., DeLano, W. L., Gros, P., Grosse-Kunstleve, R. W., Jiang, J. S., Kuszewski, J., Nilges, M., Pannu, N. S., Read, R. J., Rice, L. M., Simonson, T., and Warren, G. L. (1998) Crystallography & NMR system: A new software suite for macromolecular structure determination, *Acta Crystallogr., Sect. D: Biol. Crystallogr. 54*, 905−921.
31. Baedeker, M., and Schulz, G. E. (2002) Structures of two histidine ammonia-lyase modifications and implications for the catalytic mechanism, *Eur. J. Biochem. 269*, 1790−1797.
32. Baedeker, M., and Schulz, G. E. (2002) Autocatalytic peptide cyclization during chain folding of histidine ammonia-lyase, *Structure 10*, 61−67.
33. Wang, L., Gamez, A., Sarkissian, C. N., Straub, M., Patch, M. G., Han, G. W., Striepeke, S., Fitzpatrick, P., Scriver, C. R., and

Stevens, R. C. (2005) Structure-based chemical modification strategy for enzyme replacement treatment of phenylketonuria, *Mol. Genet. Metab. 86*, 134−140.
34. Pilbak, S., Tomin, A., Retey, J., and Poppe, L. (2006) The essential tyrosine-containing loop conformation and the role of the C-terminal multi-helix region in eukaryotic phenylalanine ammonia-lyases, *FEBS J. 273*, 1004−1019.
35. Appert, C., Zon, J., and Amrhein, N. (2003) Kinetic analysis of the inhibition of phenylalanine ammonia-lyase by 2-aminoindan-2-phosphonic acid and other phenylalanine analogues, *Phytochemistry 62*, 415−422.
36. Watts, K. T., Mijts, B. N., Lee, P. C., Manning, A. J., and Schmidt-Dannert, C. (2006) Discovery of a substrate selectivity switch in tyrosine ammonia-lyase, a member of the aromatic amino acid lyase family, *Chem. Biol. 13*, 1317−1326.

BI7003685